PAPER

Check for updates

1,4-Azaborine based unfused non-fullerene acceptors for organic solar cells†

Shihao Chen,‡[a] Minghao Dong,‡[a] Yuanqing Bai,[a] Yuting Chen,[a] Yuang Fu,[b] Lin Shao,[a] Xinhui Lu,[b] Chunchen Liu, [ID] *[a] Kai Zhang, [ID] [a] Hongbin Wu [ID] [a] and Fei Huang [ID] *[a]

1,4-Azaborine, containing both boron and nitrogen in an aromatic hydrocarbon, displays unique electronic properties compared with its all-carbon analogue and shows great potential as a multiresonant thermally activated delayed fluorescence material. However, conjugated molecules featuring 1,4-azaborine for organic solar cells (OSCs) have not yet been explored. In this study, two novel acceptor–donor– acceptor (A–D–A) conjugated molecules, **ABBT-BO** and **ABBT-DT**, using dithieno-1,4-azaborine as the core D unit have been designed and synthesized. Both molecules exhibited excellent solubility, strong and broad absorption and appropriate energy levels, enabling them to be promising candidates for non-fullerene acceptors (NFAs). It was found that the shorter alkyl chain of **ABBT-BO** could endow the device with superior morphology, resulting in more sufficient exciton dissociation, improved carrier transport and suppressed charge recombination. Impressively, PM6:**ABBT-BO** based OSCs achieved a power conversion efficiency (PCE) of 10.07% with an open-circuit voltage (V_{OC}) of 0.900 V, a short-circuit current density (J_{SC}) of 16.41 mA cm^{-2}, and a fill factor (FF) of 68.16%, which is the highest efficiency reported for NFAs featuring BN-heteroarenes. This work demonstrates the significant potential of 1,4-BN-heteroarenes for constructing novel NFAs toward high-performance OSCs.

Introduction

Organic solar cells (OSCs), as a promising renewable energy technology, have attracted great attention due to their distinct advantages of light weight, flexibility, semitransparency and solution processability.[1–6] In the past few decades, great efforts have been devoted to exploring various photoactive materials to promote the power conversion efficiency (PCE) of OSCs.[7–13] In the past few years, the PCE of OSCs has soared to 19% mainly owing to the discovery of small molecule non-fullerene acceptors (NFAs).[14,15] In contrast to the fullerene acceptors, NFAs possessed strong near-infrared (NIR) absorption and easy structure-modification and readily tuned electronic energy levels.[16,17] Nowadays, a lot of attention has been paid to the structure optimization of typical NFAs of ITIC and Y6 derivatives, whereas NFAs based on novel conjugated backbones lack exploration.[18] Therefore, it is of significance to design and synthesize appealing heteroarenes for constructing novel NFAs toward high-performance OSCs.[19–22]

BN-heteroarenes, which employ both boron and nitrogen in aromatic hydrocarbons, display unique electronic properties compared with their all-carbon analogues and have shown great potential for applications in organic electronics.[23] Boron and nitrogen atoms can form a B←N coordinate bond or a B–N covalent bond (Fig. 1a).[24] BN-heteroarenes embedded with a B←N coordinate bond exhibit an electron-deficient nature because of the positive charge of the nitrogen atom, which thus has been widely utilized for constructing various polymer and small molecule acceptors in OSCs.[25–27] Meanwhile, BN-heteroarenes featuring a B–N covalent bond are also competitive candidates for constructing conjugated materials for organic electronics.[28] Azaborines is the basic B–N covalent heteroarene, where two carbon atoms are respectively replaced with boron and nitrogen atoms. According to the relative positions of B and N atoms, azaborines are classified as three isomers: 1,2-azaborine, 1,3-azaborine and 1,4-azaborine (Fig. 1a). Due to its worst thermodynamic stability, conjugated polymers/molecules containing 1,3-azaborine have not yet been explored.[29] Very recently, Duan and co-workers successfully employed 1,2-azaborine to construct polymer donor and small molecule NFAs for OSCs, and considerable device performances were achieved.[30,31]

Compared with its 1,2- and 1,3-isomers, 1,4-azaborine exhibits moderate thermodynamic stability[32] and some unique

[a] State Key Laboratory of Luminescent Materials and Devices, Institute of Polymer Optoelectronic Materials and Devices, School of Materials Science and Engineering, South China University of Technology, Guangzhou, 510640, P. R. China. E-mail: mscliu@scut.edu.cn; msfhuang@scut.edu.cn

[b] Department of Physics, The Chinese University of Hong Kong, New Territories, Hong Kong 999077, China

† Electronic supplementary information (ESI) available. See DOI: https://doi.org/10.1039/d2ta09188g

‡ S. Chen and M. Dong contributed equally to this work.

This journal is © The Royal Society of Chemistry 2023

J. Mater. Chem. A, 2023, **11**, 3653–3662 | **3653**

Fig. 1 (a) The classification of BN-heteroarenes featuring azaborines. (b) Chemical structures of **PM6**, **ABBT-BO** and **ABBT-DT**. (c) Schematic energy diagram of **PM6**, **ABBT-BO** and **ABBT-DT**. (d) Normalized absorption spectra in chloroform solution. (e) Normalized absorption spectra of neat films.

electronic properties due to the different π-electron distributions and dipole moments.[29] Since the first 1,4-azaborine-containing anthracene was reported in 1961,[33] numerous 1,4-BN-heteroarenes have been designed and synthesized. In particular, π-extended conjugated molecules featuring 1,4-azaborine have attracted great interest due to their potential in multiresonant thermally activated delayed fluorescence (MR-TADF) materials.[34–36] However, to the best of our knowledge, conjugated molecules featuring 1,4-azaborine for OSCs are still unexplored. Therefore, it is necessary to design and synthesize 1,4-BN-heteroarene based donor/acceptors for OSCs and investigate the impact of 1,4-azaborine on material properties as well as device performance.

Herein, dithieno-1,4-azaborine was used, for the first time, as the core unit to construct two novel A–D–A-type small molecule NFAs, **ABBT-BO** and **ABBT-DT** (Fig. 1a and b). The molecular skeleton exhibits good planarity because of the nearly planar structure of 1,4-azaborine and intramolecular S⋯O

noncovalent interactions. Both molecules exhibit good solubility, strong NIR absorption, and appropriate energy levels, making them competitive candidates for NFAs. As a result, OSCs with **ABBT-BO/DT** as acceptors have been successfully fabricated. It was found that the length of branched alkyl chains in the nitrogen atom of 1,4-azaborine will make a distinct difference to the exciton dissociation, carrier transport and charge recombination in devices. Eventually, the optimal **PM6:ABBT-BO** device achieved a PCE of over 10% due to its superior morphology, higher exciton dissociation, increased carrier lifetime and suppressed charge recombination. To the best of our knowledge, it is the highest performance for OSCs based on small molecule NFAs featuring BN-heteroarenes. As the first attempt to design and synthesize 1,4-BN-heteroarene based NFAs, this study may provide some inspiration for developing more BN-containing NFAs for high-performance OSCs.

3654 | J. Mater. Chem. A, 2023, **11**, 3653–3662

This journal is © The Royal Society of Chemistry 2023

Results and discussion

Materials synthesis and characterization

The synthetic routes of **ABBT-BO** and **ABBT-DT** are shown in Fig. S1 and S2.† Intermediates **2** with a butyl-octyl chain and **6** with a decyltetradecyl chain were both obtained in a one-pot palladium-catalysed Buchwald–Hartwig cross-coupling reaction with sequential formation of two C–N bonds. The incorporation of a long alkyl chain on the nitrogen atom was essential to ensure sufficient solubility for the fabrication of devices using the spin-coating method. The key intermediates **3** and **7** were then generated by a selective Friedel–Crafts-type C–H borylation from commercially available reagent PhBCl$_2$.[37] After converting compound **3** and **7** to their respective bis-tributyltin derivatives, **4** and **8**, target NFAs (**ABBT-BO** and **ABBT-DT**) were then obtained *via* a Stille coupling reaction followed by a Knoevenagel condensation reaction. Notably, the incorporation of alkoxy groups was in favor of the coplanarity of the target molecules for the conformational "locks" *via* S⋯O interactions[38,39] as well as upshifting of HOMO energy levels for a red-shifted absorption.[40] The molecular structures were thoroughly confirmed by ^{1}H/^{13}C nuclear magnetic resonance (NMR) and matrix-assisted laser desorption/ionisation time-of-flight (MALDI-TOF) analyses (Fig. S11–S22†). Both NFAs exhibited sufficient solubility in common organic solvents, such as chloroform, chlorobenzene and toluene, enabling the solution processability for neat and blend films.

Photophysical properties

The highest occupied molecular orbital (HOMO)/lowest unoccupied molecular orbital (LUMO) energy levels were measured to be $-3.97/-5.71$ eV for **ABBT-BO** and $3.97/-5.72$ eV for **ABBT-DT** by cyclic voltammetry (CV) tests (Fig. 1c and S3†). A negligible difference was observed for the electronic energy levels of these two molecules. Absorption spectra of **ABBT-BO** and **ABBT-DT** in chloroform solution and neat films are shown in Fig. 1d and e, and the corresponding data are outlined in Table 1.

The length of the branched alkyl chain in 1,4-azaborine made negligible difference to the solution absorption for **ABBT-BO** and **ABBT-DT**, both of which exhibited an identical peak located at 673 nm (Fig. 1d). Notably, both **ABBT-BO** and **ABBT-DT** exhibited a maximum absorption coefficient of over 1.40×10^5 M^{-1} cm^{-1}, (Fig. S8†) which was comparable to that of the star acceptor Y6.[41] In thin films, the absorption spectra of both molecules exhibited a red-shift over 40 nm relative to those in solution, resulting in a strong and broad absorption in the region of 500–800 nm (Fig. 1e). The **ABBT-BO** film exhibited an absorption peak at 792 nm, slightly red-shifted relative to that at 778 nm of **ABBT-DT**. Accordingly, optical bandgaps of 1.57 and 1.59 eV were deduced for **ABBT-BO** and **ABBT-DT**, respectively. The complementary absorption with **PM6** and appropriate energy levels make these two 1,4-azaborine-containing molecules competitive candidates for NFAs in OSCs.

Calculated geometry and electronic properties

Density-functional theory (DFT) calculations were conducted to investigate the molecular geometry and energy levels at the B3LYP/6-311+g(d,p) level using the Gaussian 16 package. To simplify the calculations, all alkoxy and alkyl chains were respectively replaced by methoxyl and methyl groups. As shown in Fig. 2a, the conjugated skeleton exhibited good coplanarity due to the nearly planar 1,4-azaborine and S⋯O noncovalent interactions, which might be beneficial for the intermolecular packing and thus, improving the charge mobility.[42–46] As shown in Fig. 2b, the HOMO energy level was mainly delocalized on the core dithieno-1,4-azaborine and alkoxyl thiophene moieties, whereas the LUMO energy level was distributed along the whole molecule, indicating efficient p–π* conjugation between boron atoms with adjacent thiophenes.[47] The calculated HOMO/LUMO was $-5.99/-3.94$ eV. The discrepancy between DFT calculation results and CV measurements may be derived from the intermolecular packing of **ABBT-BO**/**ABBT-DT** that was generally ignored in the calculations.[48]

The electrostatic potential (ESP) is a physical property that can reflect the static charge distribution of a molecule, and it has been usually investigated to speculate the molecular packing behaviour[49] and the exciton dissociation progress in OSCs.[50] As shown in Fig. 2c and S4,† negative ESP distributions for boron and its adjacent carbon atoms and positive distributions for nitrogen and its adjacent carbon atoms were observed, indicating the obvious dipole moment between boron and nitrogen atoms, which was similar to the ESP distribution in the core of Y-series NFAs. The negative ESP distribution at the B-side region was supposed to enhance the electron-accepting ability. Eventually, due to the incorporation of electron-deficient B atoms, these molecules displayed similar ESP distributions with Y-series NFAs[51,52] along the conjugated backbone, which was speculated to facilitate the intermolecular packing[53,54] and exciton dissociation.

Dielectric constant measurement

Organic semiconductors typically have low dielectric constants ($\varepsilon_r < 3$), resulting in high exciton binding energy of hundreds of meVs. A higher ε_r is persistently pursued for organic

Table 1 Optical and electrochemical properties of ABBT-BO and ABBT-DT

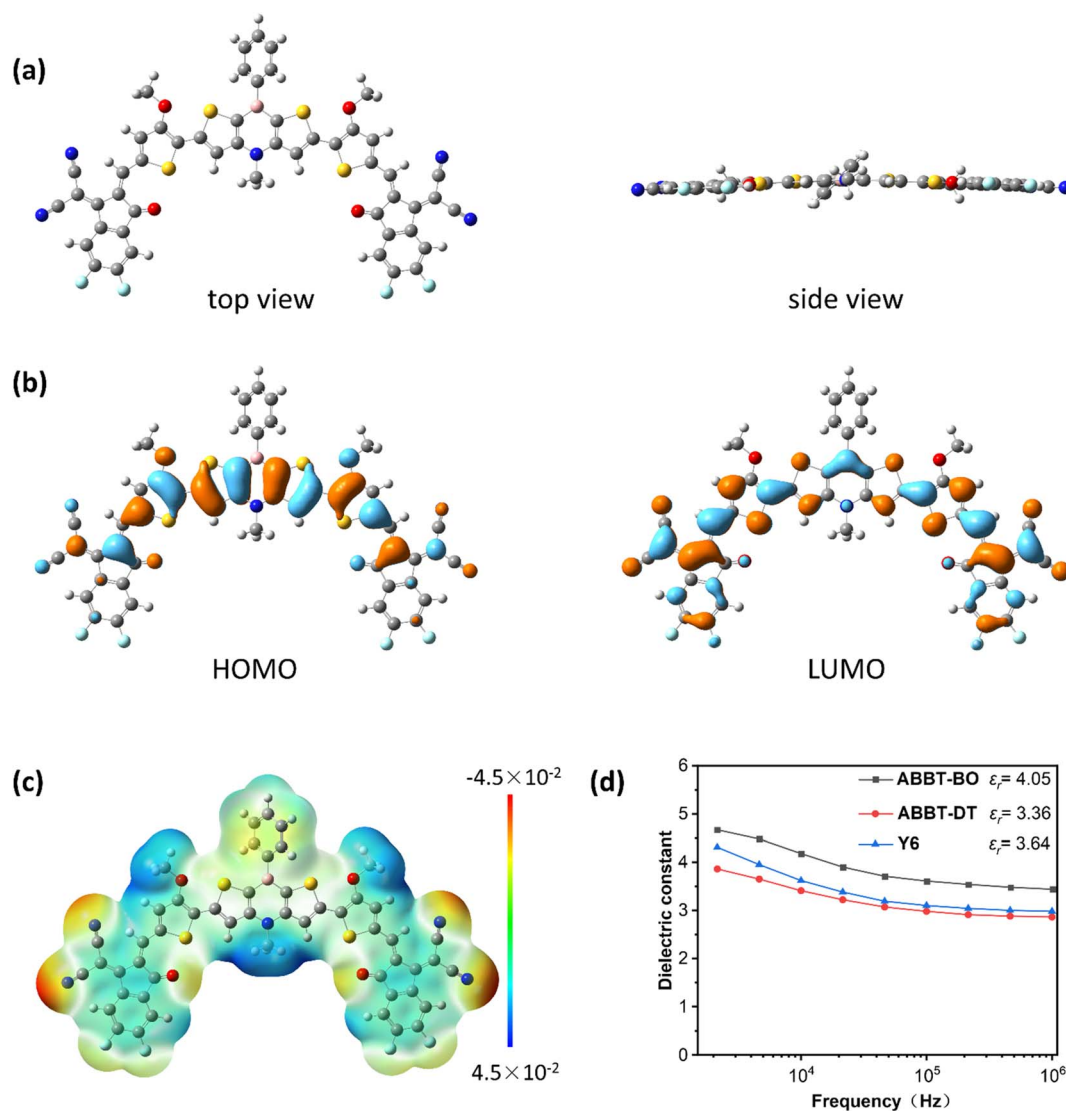| Acceptors	λ_{max} Solution	Film	λ_{onset} [film]	E_g^{opt} [eV]	E_{HOMO} [eV]	E_{LUMO} [eV]	E_g [eV]	ε [M^{-1} cm^{-1}]
ABBT-BO	673	719	792	1.57	-5.71	-3.97	1.74	1.44×10^5
ABBT-DT	673	713	778	1.59	-5.72	-3.97	1.75	1.45×10^5

Fig. 2 (a) Molecular geometries obtained by DFT calculations. (b) Calculated frontier molecular orbitals of the molecules, (c) ESP distribution on the molecular surface of the **ABBT–BO/DT** backbone. (d) Dielectric constant *versus* frequency.

semiconductors to promote exciton dissociation and charge transport accompanied by decreased geminate and non-geminate recombinations.[55] Considering the unique dipole moment and electronic properties of a 1,4-azaborine unit, the ε_r values of **ABBT-BO**, **ABBT-DT** and Y6 were measured using the parallel-plate capacitance measurement with impedance spectroscopy. The ε_r values were obtained from the equation: $C = \varepsilon_0\varepsilon_r A/d$, where C is the capacitance, ε_0 is the permittivity of free space, A is the device area, and d is the thickness of the test film. As shown in Fig. 2d, the ε_r values were plotted as a function of the frequency. Y6 showed an ε_r of 3.64, consistent with the re-ported studies.[56] A slightly lower ε_r of 3.36 was observed for **ABBT-DT**; however, **ABBT-BO** exhibited an ε_r value of 4.05, even higher than that of Y6, which was speculated to facilitate the exciton dissociation in organic electronics.[57,58] The lower dielectric constant of **ABBT-DT** may be ascribed to the longer alkyl chain that reduces the number of polarizable molecular units in a given volume.[59]

Photovoltaic performance

Photovoltaic devices were fabricated with a conventional configuration of ITO/PEDOT:PSS/**PM6:ABBT-BO** or **ABBT-DT**/PNDIT-F3N[60]/Ag. **PM6** was selected as the polymer donor due to its matched energy levels and complementary absorption with **ABBT-BO/DT**. The current density–voltage (*J*–*V*) curves of the devices are shown in Fig. 3a, and the optimized performance parameters are summarized in Table 2. The **PM6:ABBT-DT** device exhibited an open circuit voltage (V_{OC}) of 0.902 V, a short circuit current density (J_{SC}) of 12.29 mA cm^{-2} and a fill factor (FF) of 56.11%, yielding a poor PCE of 6.24%. However, the **PM6:ABBT-BO** device achieved a PCE of 10.07% with an V_{OC} of 0.900 V and a significantly higher J_{SC} of 16.41 mA cm^{-2} and FF of 68.16%. To the best of our knowledge, this is the highest PCE reported to date for small molecule NFAs featuring BN-heteroarenes.

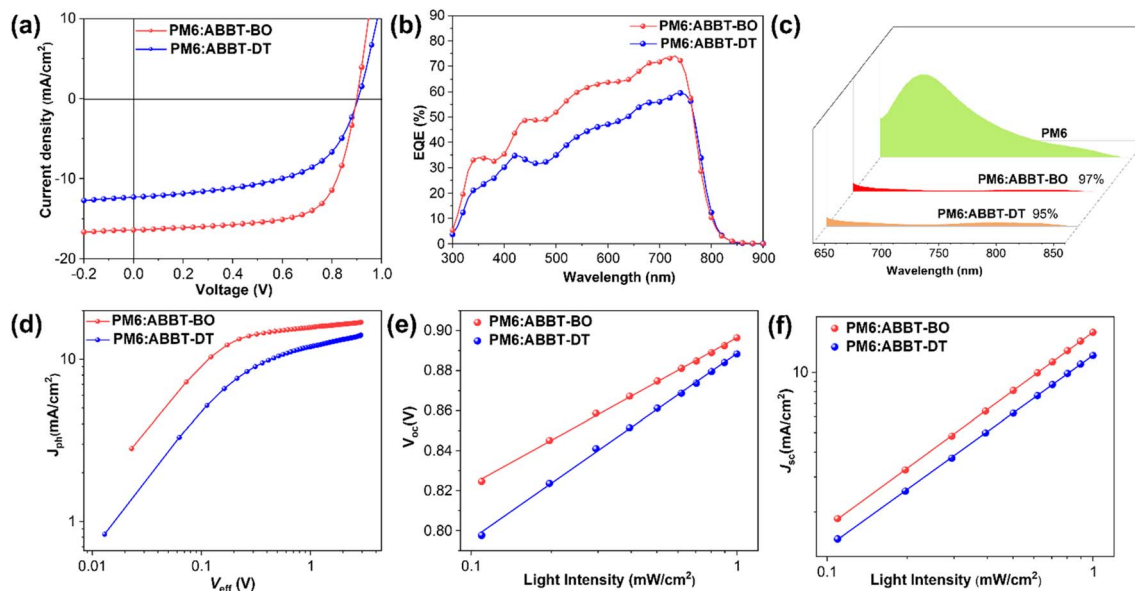**3656** | *J. Mater. Chem. A*, 2023, **11**, 3653–3662

This journal is © The Royal Society of Chemistry 2023

Fig. 3 (a) J–V characteristics and (b) EQE spectra of the optimal OSCs. (c) PL spectra of PM6 and PM6:NFA blend films. (d) J_{ph}–V_{eff} relationships of PM6:ABBT-BO and PM6:ABBT-DT. (e) V_{OC} *versus* light intensity curves and (f) J_{SC} *versus* light intensity curves of PM6:ABBT-BO and PM6:ABBT-DT.

The spectra of external quantum efficiency (EQE) are displayed in Fig. 3b. Both devices achieved a broad photo response in the region of 400–800 nm, coinciding well with the combined absorption of PM6 and ABBT-BO/DT. Impressively, a thoroughly stronger photo response was achieved for the PM6:ABBT-BO device, which was in a good agreement with its higher J_{SC}. As a result, J_{SC} values of 15.61 and 12.07 mA cm^{-2} were deduced for PM6:ABBT-BO and PM6:ABBT-DT, respectively, both of which agree well with the J_{SC} results obtained from the J–V curves (within 5% error), validating the authenticity of device data.

To elucidate the underlying mechanism for the performance difference between ABBT-BO and ABBT-DT based devices, exciton dissociation, charge recombination, carrier lifetime and transport were investigated. Photoluminescence (PL) emission spectra of neat PM6 and PM6:ABBT-BO/DT films are shown in Fig. 3c, and the PL emission of PM6 (excited at 615 nm) was largely quenched in both blend films, indicating efficient exciton dissociation at D/A interfaces. However, it should be noted that the PL quenching efficiency of the PM6:ABBT-BO film (97%) is slightly higher than that of the PM6:ABBT-DT one (95%), showing more sufficient exciton dissociation in the former film. The photocurrent density (J_{ph}) *versus* effective voltage (V_{eff}) curves were measured to gain further insight into

exciton dissociation behaviours in OSCs (Fig. 3d). The J_{ph}/J_{sat} value is defined as exciton dissociation efficiency, where J_{ph} and J_{sat} respectively represent the photogenerated and saturation current density. The J_{ph}/J_{sat} values were calculated to be 97.1% and 90.4% for PM6:ABBT-BO and PM6:ABBT-DT based devices. The higher J_{ph}/J_{sat} value of the PM6:ABBT-BO based device suggests its more efficient exciton dissociation, which is consistent with the above PL-quenching results.

The curves of J_{SC} or V_{OC} *versus* the light intensity (P_{light}) were plotted to study the recombination behaviours in ABBT-BO/DT based devices. As shown in Fig. 3e, the P_{light} dependence of the V_{OC} was fitted to reveal the trap-assisted recombination. The slope approaching $1KT/q$ means weaker trap-assisted recombination in the devices (K is the Boltzmann constant, T is the temperature in units of kelvin, and q is the elementary charge). The slopes for PM6:ABBT-BO and PM6:ABBT-DT devices were deduced to be 1.23 and $1.56KT/q$, respectively, indicating the severer trap-assisted recombination in PM6:ABBT-DT devices. Additionally, the curves of J_{SC} *versus* P_{light} were measured (Fig. 3f) to clarify the bimolecular recombination. The relationship between J_{SC} and P_{light} can be described as $J_{SC} \propto P_{light}^{\alpha}$, where α is the exponential factor which would be close to 1 when there is negligible bimolecular recombination. The slopes

Table 2 Photovoltaic parameters of the optimized solar cells based on ABBT-BO and ABBT-DT under standard AM 1.5 G illumination, 100 mW cm^{-2}

Entry	V_{OC} [V]	J_{SC} [mA cm^{-2}]	FF [%]	PCE$_{ave}$[a] [%]	PCE$_{max}$ [%]
PM6:ABBT-BO	0.900	16.41	68.16	10.02 ± 0.05	10.07
PM6:ABBT-DT	0.905	12.29	56.11	6.15 ± 0.05	6.24

[a] Average of more than 5 individual devices.

This journal is © The Royal Society of Chemistry 2023

J. Mater. Chem. A, 2023, 11, 3653–3662 | 3657

extracted for **PM6:ABBT-BO/ABBT-DT** devices were 0.974 and 0.959, respectively, indicating the weaker bimolecular recombination in the **PM6:ABBT-BO** device. The higher exciton dissociation efficiency, and lower trap-assisted and bimolecular recombination together verified the higher FF and J_{SC} for **PM6:ABBT-BO** devices.

Moreover, the Platform for All-In-One Characterization of Solar Cells and OLED (PAIOS) was used to gain insight into the charge recombination within active layers in operating devices.[61–63] The charge density for devices based on **ABBT-BO/DT** were shown as a function of bias light intensity (Fig. 4a). The charge lifetime (τ) was extracted from the transient photovoltage (TPV) decay dynamics. Obviously, at the same light intensity, the **PM6:ABBT-BO** device exhibited higher carrier density, suggesting the reduced charge recombination and thus higher photocurrent generation. Additionally, the **PM6:ABBT-BO** active layer displayed a higher τ value than its **ABBT-DT** counterpart in a wide range of light intensities (Fig. 4b). Furthermore, charge-extraction (CE) measurements were performed at various light intensities to estimate carrier densities (n) for **PM6:ABBT-BO/DT** devices(Fig. 4c). An increased n value can be obtained for the **ABBT-BO** based device, which agrees well with its higher J_{SC}. The bimolecular recombination rate constants k_{rec} were then calculated from the τ and n values according to $k_{rec} = 1/(\lambda + 1)n\tau$ (λ is the recombination order). As shown in Fig. 4d, k_{rec} for the **ABBT-DT** based device was significantly larger than that for the **ABBT-BO** based one. All of these results further revealed that the superior performance of the **ABBT-BO** based device was mainly derived from a higher carrier lifetime and density, and reduced carrier recombination.

The transient photovoltage (TPV) and transient photocurrent (TPC) decay measurements were also carried out to thoroughly understand charge properties including carrier lifetime, recombination and extraction in devices. As shown in Fig. 4d, the transient photovoltage decay lifetime of **ABBT-BO** and **ABBT-DT** based devices was 190 and 137 μs, respectively. The longer lifetime indicates the weaker premature recombination of charge carriers in the **PM6:ABBT-BO** device. The TPC measurement was conducted under short-circuit conditions, which reflects the time from charge generation to charge collection by the electrode.[64] A shorter TPC means more efficient carrier transport and extraction progress in OSCs. By fitting the TPC curves as shown in Fig. 4e, the charge extraction time was calculated to be 0.27 and 0.41 μs for **ABBT-BO** and **ABBT-DT** based devices, respectively. Overall, the results of TPV and TPC measurements indicated that the improvement of the charge transfer and collection were significantly enhanced in **ABBT-BO** based devices.

The hole (μ_h) and electron (μ_e) mobilities were also measured by the space-charge-limited-current (SCLC) method (Fig. S6 and S7†). The μ_h/μ_e of **PM6:ABBT-BO** and **PM6:ABBT-DT** devices were 7.20/5.38 $\times$ 10^{-5}, and 5.16/3.52 $\times$ 10^{-5} cm^2 V^{-1} s^{-1}, respectively. Accordingly, the μ_h/μ_e ratio of 1.34 and 1.47 were calculated for **PM6:ABBT-BO** and **PM6:ABBT-DT** devices, respectively. Apparently, **PM6:ABBT-BO** based devices exhibited higher and more balanced charge transport, contributing to its higher FF and J_{SC}.

Moreover, energy losses (E_{loss}) in **ABBT-BO** and **ABBT-DT** based devices were measured by using the Fourier-transform photocurrent spectrum (FTPS) (Fig. S9†).[65] In general, E_{loss} in
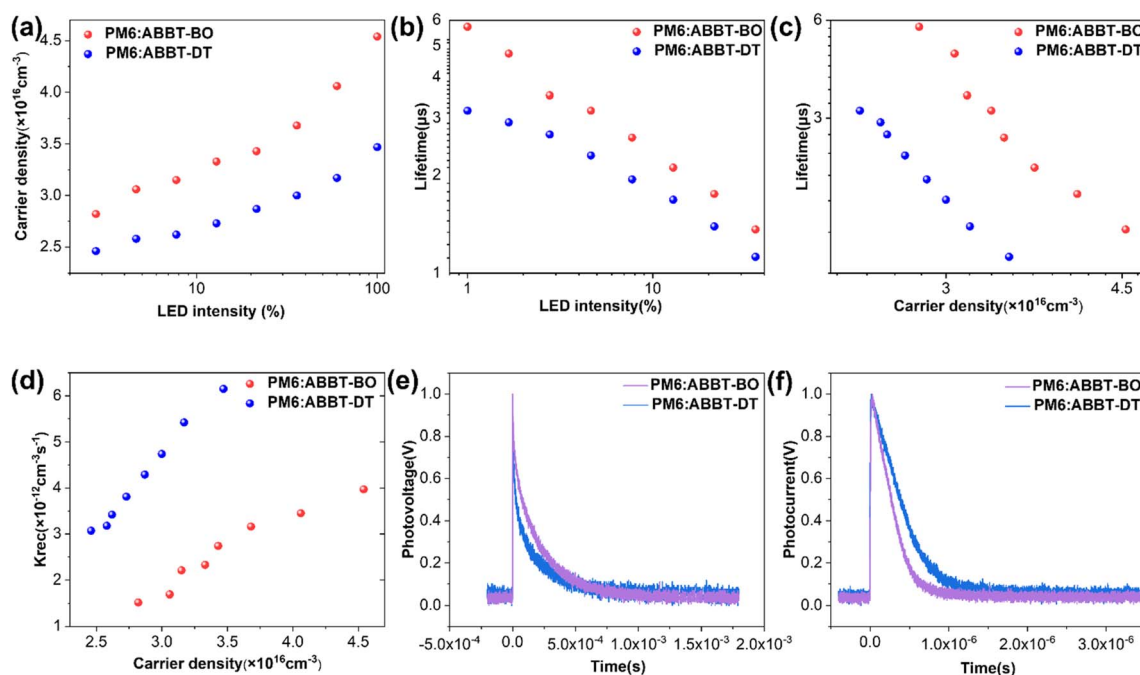

Fig. 4 (a) Charge density *versus* light intensity. (b) The carrier lifetimes and densities under different illumination intensities. (c) Charge lifetime *versus* charge density. (d) Bimolecular recombination rate constant k_{rec} extracted from τ and n. (e) TPV and (f) TPC characterization of PM6:ABBT-BO and PM6:ABBT-DT.

3658 | *J. Mater. Chem. A*, 2023, **11**, 3653–3662

This journal is © The Royal Society of Chemistry 2023

solar cells can be divided three parts: (1) ΔE_1 is the intrinsic radiative recombination loss in the Shockley–Queisser limit, which is inevitable for all photovoltaic cells. (2) ΔE_2 is the additional radiative recombination energy loss, originating from the extra absorption within the bandgap active layer in BHJ OSCs. (3) ΔE_3 results from the non-radiative recombination at the D/A interface in OSCs. As shown in Table S1,† the incorporation of different alkyl side chains showed weak impacts on E_{loss}. Unfortunately, a relatively high value of over 0.70 eV was calculated for both **ABBT-BO** and **ABBT-DT** based devices compared to Y6 based devices, which probably resulted in the inferior J_{sc} and FF of the **ABBT-BO/DT** based device relative to the state-of-the-art devices.

Morphology

It is well recognised that the nanoscale morphology of the active layers is intimately connected with the exciton dissociation, charge transport and recombination in OSCs.[66] Transmission electron microscopy (TEM) and atomic force microscopy (AFM) results were obtained as shown in Fig. 5. The homogeneously distributed nanofiber microstructures in the **PM6:ABBT-BO** film were supposed to be favourable for exciton dissociation and charge transport. In contrast, obvious island-like agglomeration could be observed in the **PM6:ABBT-DT** film, leading to oversized phase separation caused by the ordered packing of the longer alkyl chain in **ABBT-DT** as reported in previous studies.[67,68] As shown in the AFM images, the **PM6:ABBT-BO** film showed a smoother top surface compared to the

PM6:ABBT-DT film. A root-mean-square roughness (R_q) of 2.54 nm was observed for the **PM6:ABBT-BO** film, remarkably larger than 6.07 nm for the **PM6:ABBT-DT** one. The superior blend morphology of **PM6:ABBT-BO** was supposed to facilitate exciton dissociation, charge transport and eventually improve the device performance.

The Flory–Huggins interaction parameters (χ) were calculated to investigate the miscibility of **PM6** with **ABBT-BO** and **ABBT-DT** (Fig. S23 and Table S3†). According to the equation: $\chi_{DA} = K(\sqrt{\gamma_D} - \sqrt{\gamma_A})^2$, where K is a constant, γ is the surface energy, and D and A refer to donor and acceptor, respectively. The χ parameters were calculated to be 0.10 K and 0.28 K for **PM6:ABBT-BO** and **PM6:ABBT-DT**, respectively. The higher χ parameter of **PM6** and **ABBT-DT** prefers to form oversized phase separation, which is consistent with the TEM and AFM images.

Grazing-incidence wide angle X-ray scattering (GIWAXS) was performed to reveal the intermolecular packing of **ABBT-BO/DT** films as well as **PM6:ABBT-BO/DT** films. Their 2D-GIWAXS patterns and line-cut profiles are presented in Fig. 6 and S9.† For the neat films, **PM6** had reflections at approximately 0.99 Å^{-1} in the out-of-plane (OOP) direction and a weak lamellar stacking peak at approximately 0.30 Å^{-1} in the in-plane (IP) direction (Table S2†). The π–π stacking peak could be attributed to the reflection at 1.74 Å^{-1} in the OOP direction, with a d-spacing of 3.22 Å. However, there were weak π–π stacking peaks but strong lamellar stacking peaks at approximately 0.33 Å in the OOP direction for both **ABBT-BO** and **ABBT-DT** neat films,

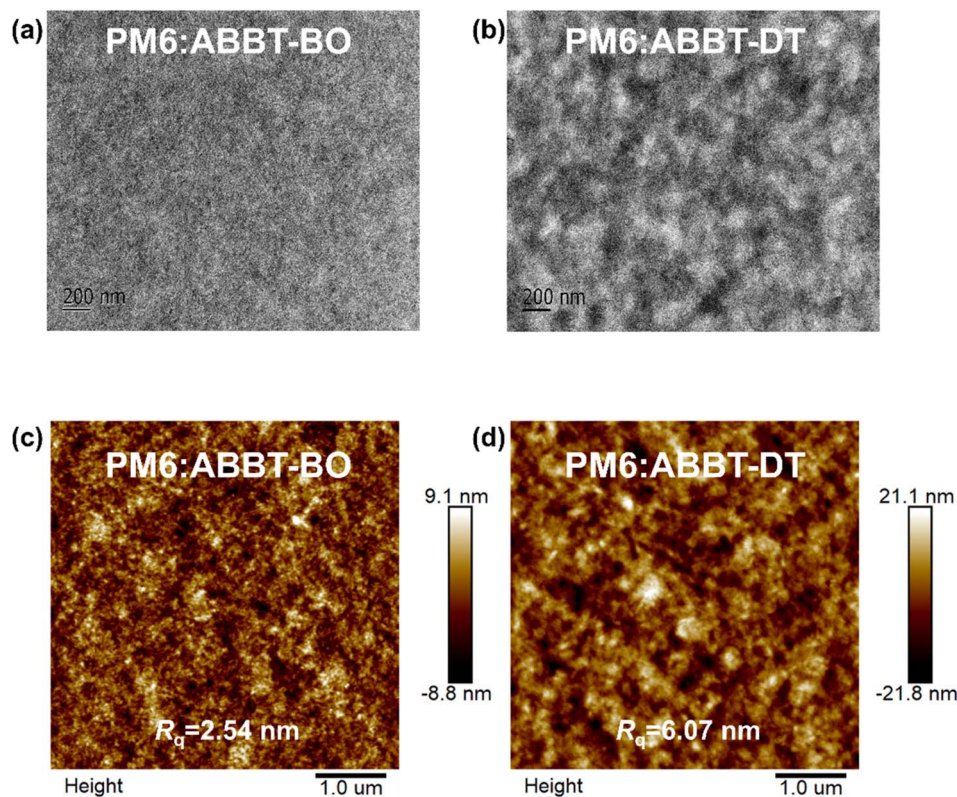**Fig. 5** (a and b) TEM height images and (c and d) AFM images of **PM6:ABBT-BO** and **PM6:ABBT-DT**.
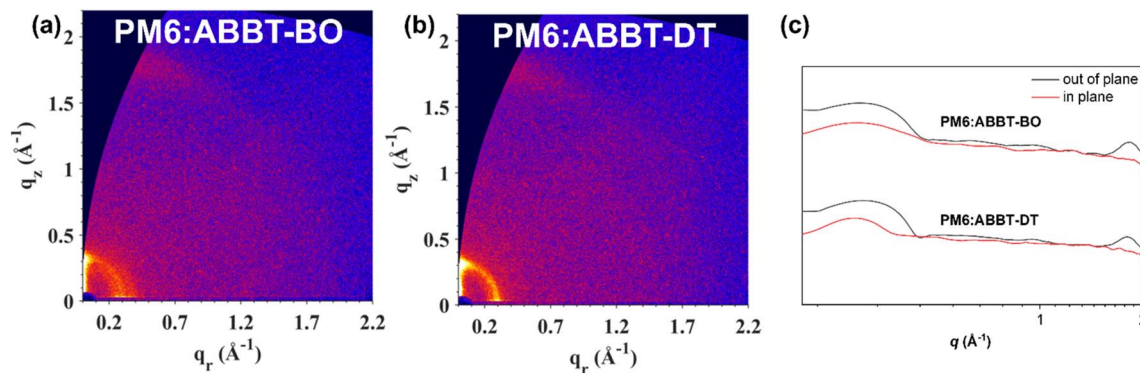
Fig. 6 2D GIWAXS patterns of (a) **PM6:ABBT-BO**, (b) **PM6:ABBT-DT** and (c) the corresponding out-of-plane (black lines) and in-plane (red lines) line cuts.

indicating the random intermolecular packing mode. For the blend films, the alkyl-to-alkyl lamellar packing in the OOP direction plays a crucial and decisive role in determining the crystalline structure. The π–π stacking peaks of the **PM6:ABBT-BO** and **PM6:ABBT-DT** films were located at 1.83 and 1.80 Å^{-1} in the OOP direction, with a d-spacing of 3.07 and 3.12 Å, respectively. The stronger and intensive π–π stacking peaks indicated that the incorporation of **PM6** enhanced the crystallinity of blend films. The crystal coherence length (CCL), which is closely related to the charge transport and device performance, was extracted from the GIWAXS line profiles. The CCL was calculated to be 21.97, 32.50 and 32.84 Å for the π–π stacking peaks located at approximately 1.80 Å^{-1} for **PM6**, **PM6:ABBT-BO** and **PM6:ABBT-DT**, respectively. The longer CCL of blends films indicates that more ordered domains and tighter π–π stacking were formed, which was beneficial for the charge transport and reduced charge recombination.

Conclusions

In summary, dithieno-fused 1,4-azaborine was innovatively used for constructing two novel A–D–A structural molecules, **ABBT-BO** and **ABBT-DT**. These molecules possessed desired solubility, broad absorption, appropriate energy levels, unique ESP distribution, high dielectric coefficient and coplanar conformation, making them promising candidates for NFAs. The OSCs with **PM6** as the donor and **ABBT-BO/DT** as acceptors have been successfully fabricated, and it was found that the length of branched alkyl chains in 1,4-azaborine could make a significant difference to the device performance. Impressively, the **ABBT-BO** based OSC achieved an optimal PCE of 10.07% with a V_{OC} of 0.900 V, a J_{SC} of 16.41 mA cm^{-2} and an FF of 68.16%. To the best of our knowledge, it is the highest efficiency reported for OSCs with small molecule NFAs featuring BN-heteroarenes. Deep investigations revealed that the superior performance of the **ABBT-BO** based device was derived from the improved exciton dissociation, higher and more balanced carrier mobility, and reduced recombination. This study sheds some light on designing novel NFAs featuring 1,4-azaborine for high-performance OSCs.

Author contributions

Shihao Chen designed and synthesised the molecules, conducted the experiments and drafted the original manuscript. Minghao Dong fabricated the organic solar cells and contributed to the data analyses. Yuanqing Bai contributed to the theoretical calculations. Yuting Chen and Hongbin Wu carried out the energy loss measurement. Yuang Fu and Xinhui Lu performed the GIWAXS measurement. Lin Shao helped in data curation. Kai Zhang helped in device data analyses. Chunchen Liu and Fei Huang guided and supervised the whole project. All authors discussed the results and commented on the manuscript.

Conflicts of interest

The authors declare no conflicts of interest.

Acknowledgements

References

1 G. Zhang, J. Zhao, P. C. Y. Chow, K. Jiang, J. Zhang, Z. Zhu, J. Zhang, F. Huang and H. Yan, *Chem. Rev.*, 2018, **118**, 3447.

2 R. Sun, Q. Wu, J. Guo, T. Wang, Y. Wu, B. Qiu, Z. Luo, W. Yang, Z. Hu, J. Guo, M. Shi, C. Yang, F. Huang, Y. Li and J. Min, *Joule*, 2020, **4**, 407.

3 S. Dong, T. Jia, K. Zhang, J. Jing and F. Huang, *Joule*, 2020, **4**, 2004.

4 Z. Hu, J. Wang, X. Ma, J. Gao, C. Xu, X. Wang, X. Zhang, Z. Wang and F. Zhang, *J. Mater. Chem. A*, 2021, **9**, 6797.

3660 | *J. Mater. Chem. A*, 2023, **11**, 3653–3662

This journal is © The Royal Society of Chemistry 2023

5 W. Liu, S. Xu, H. Lai, W. Liu, F. He and X. Zhu, *CCS Chem.*, 2022, 1.

6 X. Meng, Z. Xing, X. Hu and Y. Chen, *Chin. J. Polym. Sci.*, 2022, **40**, 1522.

7 C. Yan, S. Barlow, Z. Wang, H. Yan, A. K. Y. Jen, S. R. Marder and X. Zhan, *Nat. Rev. Mater.*, 2018, **3**, 18003.

8 Q. Wei, W. Liu, M. Leclerc, J. Yuan, H. Chen and Y. Zou, *Sci. China: Chem.*, 2020, **63**, 1352.

9 C. Sun, F. Pan, H. Bin, J. Zhang, L. Xue, B. Qiu, Z. Wei, Z.-G. Zhang and Y. Li, *Nat. Commun.*, 2018, **9**, 743.

10 Q. Liu, Y. Jiang, K. Jin, J. Qin, J. Xu, W. Li, J. Xiong, J. Liu, Z. Xiao, K. Sun, S. Yang, X. Zhang and L. Ding, *Sci. Bull.*, 2020, **65**, 272.

11 S. Chen, L. Feng, T. Jia, J. Jing, Z. Hu, K. Zhang and F. Huang, *Sci. China: Chem.*, 2021, **64**, 1192.

12 P. Han, M. Lin, Q. Jiang, H. Ning, M. Su, L. Dang, F. He and Q. Wu, *CCS Chem.*, 2022, 1.

13 L. Ye, W. Ye and S. Zhang, *J. Semicond.*, 2021, **42**, 101607.

14 P. Bi, S. Zhang, Z. Chen, Y. Xu, Y. Cui, T. Zhang, J. Ren, J. Qin, L. Hong, X. Hao and J. Hou, *Joule*, 2021, **5**, 2408.

15 Y. Cui, Y. Xu, H. Yao, P. Bi, L. Hong, J. Zhang, Y. Zu, T. Zhang, J. Qin, J. Ren, Z. Chen, C. He, X. Hao, Z. Wei and J. Hou, *Adv. Mater.*, 2021, **33**, 2102420.

16 Y. Liu, B. Liu, C.-Q. Ma, F. Huang, G. Feng, H. Chen, J. Hou, L. Yan, Q. Wei, Q. Luo, Q. Bao, W. Ma, W. Liu, W. Li, X. Wan, X. Hu, Y. Han, Y. Li, Y. Zhou, Y. Zou, Y. Chen, Y. Li, Y. Chen, Z. Tang, Z. Hu, Z.-G. Zhang and Z. Bo, *Sci. China: Chem.*, 2022, **65**, 224.

17 C. Liu, Y. Bai, Z. Hu and F. Huang, *Sci. Sin.: Chim.*, 2022, **52**, 1948.

18 C. Cui, *Acta Polym. Sin.*, 2021, **52**, 663.

19 F. Huang, Z. Li, G. Song, C. Jiang, Y. Yang, J. Wang, X. Wan, C. Li, Z. Yao and Y. Chen, *Adv. Funct. Mater.*, 2022, 2211140.

20 S. Li, L. Zhan, F. Liu, J. Ren, M. Shi, C.-Z. Li, T. P. Russell and H. Chen, *Adv. Mater.*, 2018, **30**, 1705208.

21 H. Huang, Q. Guo, S. Feng, C. e. Zhang, Z. Bi, W. Xue, J. Yang, J. Song, C. Li, X. Xu, Z. Tang, W. Ma and Z. Bo, *Nat. Commun.*, 2019, **10**, 3038.

22 X. Liao, W. Xie, Z. Han, Y. Cui, X. Xia, X. Shi, Z. Yao, X. Xu, X. Lu and Y. Chen, *Adv. Funct. Mater.*, 2022, **32**, 2204255.

23 Z. X. Giustra and S.-Y. Liu, *J. Am. Chem. Soc.*, 2018, **140**, 1184.

24 J. Miao, Y. Wang, J. Liu and L. Wang, *Chem. Soc. Rev.*, 2022, **51**, 153.

25 C. Dou, J. Liu and L. Wang, *Sci. China: Chem.*, 2017, **60**, 450.

26 M. M. Morgan, M. Nazari, T. Pickl, J. M. Rautiainen, H. M. Tuononen, W. E. Piers, G. C. Welch and B. S. Gelfand, *Chem. Commun.*, 2019, **55**, 11095.

27 F. Liu, J. Liu and L. Wang, *Org. Chem. Front.*, 2019, **6**, 1996.

28 T. Hatakeyama, K. Shiren, K. Nakajima, S. Nomura, S. Nakatsuka, K. Kinoshita, J. Ni, Y. Ono and T. Ikuta, *Adv. Mater.*, 2016, **28**, 2777.

29 C. Chen, C.-Z. Du and X.-Y. Wang, *Adv. Sci.*, 2022, **9**, 2200707.

30 S. Pang, Z. Wang, X. Yuan, L. Pan, W. Deng, H. Tang, H. Wu, S. Chen, C. Duan, F. Huang and Y. Cao, *Angew. Chem., Int. Ed.*, 2021, **60**, 8813.

31 X. Liu, S. Pang, L. Zeng, W. Deng, M. Yang, X. Yuan, J. Li, C. Duan, F. Huang and Y. Cao, *Chem. Commun.*, 2022, **58**, 8686.

32 M. Baranac-Stojanović, *Chem.–Eur. J.*, 2014, **20**, 16558.

33 P. M. Maitlis, *J. Chem. Soc.*, 1961, 425.

34 T. Huang, W. Jiang and L. Duan, *J. Mater. Chem. C*, 2018, **6**, 5577.

35 P. Jiang, J. Miao, X. Cao, H. Xia, K. Pan, T. Hua, X. Lv, Z. Huang, Y. Zou and C. Yang, *Adv. Mater.*, 2022, **34**, 2106954.

36 T. Wang, Y. Zou, Z. Huang, N. Li, J. Miao and C. Yang, *Angew. Chem., Int. Ed.*, 2022, **61**, e202211172.

37 K. Mitsudo, K. Shigemori, H. Mandai, A. Wakamiya and S. Suga, *Org. Lett.*, 2018, **20**, 7336.

38 Y. Liu, Z. Zhang, S. Feng, M. Li, L. Wu, R. Hou, X. Xu, X. Chen and Z. Bo, *J. Am. Chem. Soc.*, 2017, **139**, 3356.

39 Z. Yao, Z. Li, S. Li, J. Xiang, X. Xia, X. Lu, M. Shi and H. Chen, *ACS Appl. Energy Mater.*, 2021, **4**, 819.

40 J. Lee, S.-J. Ko, H. Lee, J. Huang, Z. Zhu, M. Seifrid, J. Vollbrecht, V. V. Brus, A. Karki, H. Wang, K. Cho, T.-Q. Nguyen and G. C. Bazan, *ACS Energy Lett.*, 2019, **4**, 1401.

41 J. Yuan, Y. Zhang, L. Zhou, G. Zhang, H.-L. Yip, T.-K. Lau, X. Lu, C. Zhu, H. Peng, P. A. Johnson, M. Leclerc, Y. Cao, J. Ulanski, Y. Li and Y. Zou, *Joule*, 2019, **3**, 1140.

42 S. Feng, M. Li, N. Tang, X. Wang, H. Huang, G. Ran, Y. Liu, Z. Xie, W. Zhang and Z. Bo, *ACS Appl. Mater. Interfaces*, 2020, **12**, 4638.

43 H. Huang, L. Yang, A. Facchetti and T. J. Marks, *Chem. Rev.*, 2017, **117**, 10291.

44 Z.-P. Yu, Z.-X. Liu, F.-X. Chen, R. Qin, T.-K. Lau, J.-L. Yin, X. Kong, X. Lu, M. Shi, C.-Z. Li and H. Chen, *Nat. Commun.*, 2019, **10**, 2152.

45 H. Huang, Z. Chen, R. P. Ortiz, C. Newman, H. Usta, S. Lou, J. Youn, Y.-Y. Noh, K.-J. Baeg, L. X. Chen, A. Facchetti and T. Marks, *J. Am. Chem. Soc.*, 2012, **134**, 10966.

46 X. Zhang, L. Qin, J. Yu, Y. Li, Y. Wei, X. Liu, X. Lu, F. Gao and H. Huang, *Angew. Chem., Int. Ed.*, 2021, **60**, 12475.

47 Y. Yu, B. Meng, F. Jäkle, J. Liu and L. Wang, *Chem.–Eur. J.*, 2020, **26**, 873.

48 Y. Chen, H. Meng, L. Ding, J. Tang, J. Yi, J. Zhang, Z. Wang, R. Ma, Z. Li, L. Lyu, X. Xu, R. Li, Q. Peng, H. Yan and H. Hu, *Chem. Mater.*, 2022, **34**, 10144.

49 J.-H. Dou, Y.-Q. Zheng, Z.-F. Yao, Z.-A. Yu, T. Lei, X. Shen, X.-Y. Luo, J. Sun, S.-D. Zhang, Y.-F. Ding, G. Han, Y. Yi, J.-Y. Wang and J. Pei, *J. Am. Chem. Soc.*, 2015, **137**, 15947.

50 H. Yao, D. Qian, H. Zhang, Y. Qin, B. Xu, Y. Cui, R. Yu, F. Gao and J. Hou, *Chin. J. Chem.*, 2018, **36**, 491.

51 C. Li, X. Gu, Z. Chen, X. Han, N. Yu, Y. Wei, J. Gao, H. Chen, M. Zhang, A. Wang, J. Zhang, Z. Wei, Q. Peng, Z. Tang, X. Hao, X. Zhang and H. Huang, *J. Am. Chem. Soc.*, 2022, **144**, 14731.

52 X. Song, K. Zhang, R. Guo, K. Sun, Z. Zhou, S. Huang, L. Huber, M. Reus, J. Zhou, M. Schwartzkopf, S. V. Roth, W. Liu, Y. Liu, W. Zhu and P. Müller-Buschbaum, *Adv. Mater.*, 2022, **34**, 2200907.

53 B. Yurash, D. Leifert, G. N. M. Reddy, D. X. Cao, S. Biberger, V. V. Brus, M. Seifrid, P. J. Santiago, A. Köhler, B. F. Chmelka, G. C. Bazan and T.-Q. Nguyen, *Chem. Mater.*, 2019, **31**, 6715.

This journal is © The Royal Society of Chemistry 2023

J. Mater. Chem. A, 2023, **11**, 3653–3662 | **3661**

54 A. J. Stephens, R. Scopelliti, F. F. Tirani, E. Solari and K. Severin, *ACS Mater. Lett.*, 2019, **1**, 3.

55 N. Cho, C. W. Schlenker, K. M. Knesting, P. Koelsch, H.-L. Yip, D. S. Ginger and A. K. Y. Jen, *Adv. Energy Mater.*, 2014, **4**, 1301857.

56 T. Li, K. Wang, G. Cai, Y. Li, H. Liu, Y. Jia, Z. Zhang, X. Lu, Y. Yang and Y. Lin, *JACS Au*, 2021, **1**, 1733.

57 X. Liu, B. Xie, C. Duan, Z. Wang, B. Fan, K. Zhang, B. Lin, F. J. M. Colberts, W. Ma, R. A. J. Janssen, F. Huang and Y. Cao, *J. Mater. Chem. A*, 2018, **6**, 395.

58 W. Gao, H. Fu, Y. Li, F. Lin, R. Sun, Z. Wu, X. Wu, C. Zhong, J. Min, J. Luo, H. Y. Woo, Z. Zhu and A. K. Y. Jen, *Adv. Energy Mater.*, 2021, **11**, 2003177.

59 P. K. Tapaswi, M.-C. Choi, Y. S. Jung, H. J. Cho, D. J. Seo and C.-S. Ha, *J. Polym. Sci., Part A: Polym. Chem.*, 2014, **52**, 2316.

60 Z. Wu, C. Sun, S. Dong, X.-F. Jiang, S. Wu, H. Wu, H.-L. Yip, F. Huang and Y. Cao, *J. Am. Chem. Soc.*, 2016, **138**, 2004.

61 Y. Firdaus, L. P. Maffei, F. Cruciani, M. A. Müller, S. Liu, S. Lopatin, N. Wehbe, G. O. N. Ndjawa, A. Amassian, F. Laquai and P. M. Beaujuge, *Adv. Energy Mater.*, 2017, **7**, 1700834.

62 R. Hamilton, C. G. Shuttle, B. O'Regan, T. C. Hammant, J. Nelson and J. R. Durrant, *J. Phys. Chem. Lett.*, 2010, **1**, 1432.

63 J. Yan, Q. Liang, K. Liu, J. Miao, H. Chen, S. Liu, Z. He, H. Wu, J. Wang and Y. Cao, *ACS Energy Lett.*, 2017, **2**, 14.

64 X. Zhou, X. Li, Y. Yan, F. Zhang, J. Zhou, T. Lin, Y. Zhu and D. Xu, *Sol. RRL*, 2022, **6**, 2200424.

65 S. Liu, J. Yuan, W. Deng, M. Luo, Y. Xie, Q. Liang, Y. Zou, Z. He, H. Wu and Y. Cao, *Nat. Photonics*, 2020, **14**, 300.

66 S. Chen, L. Hong, M. Dong, W. Deng, L. Shao, Y. Bai, K. Zhang, C. Liu, H. Wu and F. Huang, *Angew. Chem., Int. Ed.*, 2023, **135**, e202213869.

67 Z. Abbas, S. U. Ryu, M. Haris, C. E. Song, H. K. Lee, S. K. Lee, W. S. Shin, T. Park and J.-C. Lee, *Nano Energy*, 2022, **101**, 107574.

68 Y. Fu, L. Wang, C. Guo, D. Li, J. Cai, B. Zhou, C. Chen, C. Liu, D. Liu, W. Li and T. Wang, *ACS Mater. Lett.*, 2022, **4**, 2009.